Chapter 5

Synthesis, mechanical, electrical, polarization induced antibacterial and cellular response of 45S5 BG - NKN composite

This chapter describes the effect of incorporation of varying amounts (0 – 30 vol. %) of piezoelectric NKN secondary phase in 45S5 bioglass on mechanical, dielectric and electrical, antibacterial and cellular functionality of 45S5 bioglass. The chapter starts with phase evolution of sintered samples using XRD and FTIR techniques. Mechanical properties such as hardness, fracture toughness, flexural and compressive strength were measured for optimally sintered composite samples. The dielectric and electrical measurement (dielectric constant, loss ac conductivity and impedance analyses) of the processed composite reveal the similar behavior to that of the natural bone. The effect of polarization induced charge and external electric field on antibacterial and cellular response has been discussed, while cells are cultured on the developed composites.

5.1 Phase evolution

X-Ray diffraction (XRD) patterns of the sintered specimen for pure BG, NKN and BG – (10 – 30) NKN composites are shown in Fig. 5.1. XRD pattern of sintered base BG specimen confirms the formation of hexagonal crystalline phase of sodium calcium silicate (#79-1088). XRD pattern of NKN also confirms the formation of phase pure $Na_{0.5}K_{0.5}NbO_3$ (#77-0038). XRD patterns of the BG– (10 - 30) NKN composites suggest that there is no dissociation of BG and NKN phases as well as any reaction between BG and NKN phases has not taken place [Fig.5.1].

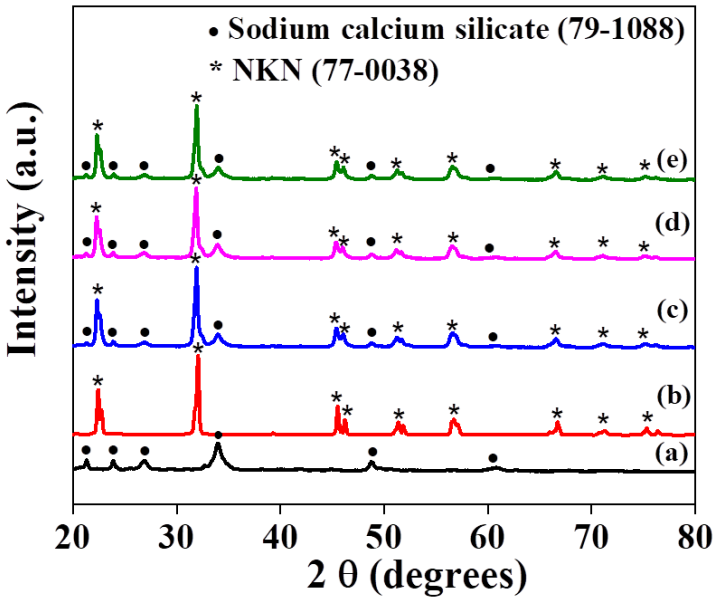

Fig. 5.1 X-Ray diffraction patterns for sintered (a) 45S5 BG, (b) NKN, (c) BG - 10 NKN, (d) BG - 20 NKN and (e) BG - 30 NKN composite samples.

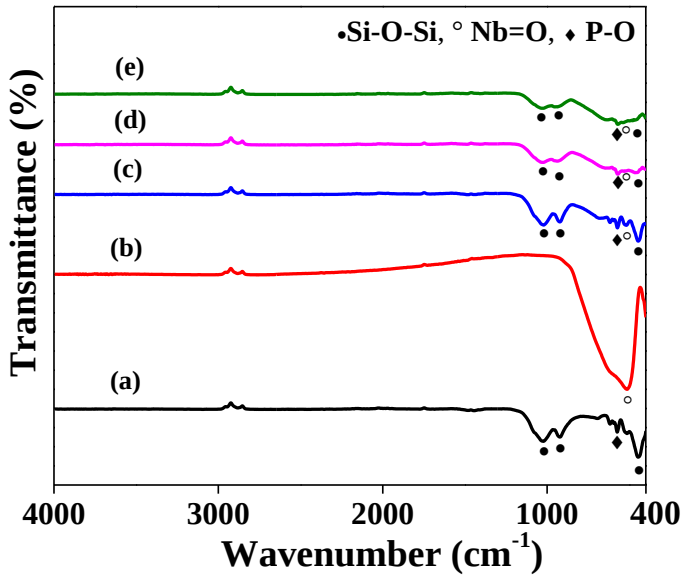

Fig. 5.2 Fourier transform infra-red (FTIR) spectra for sintered (a) 45S5 BG, (b) NKN, (c) BG - 10 NKN, (d) BG - 20 NKN and (e) BG - 30 NKN composite samples.

FTIR analyses of the BG sample reveal the characteristic vibrational bands of BG at ~ 450 cm^{-1}, 939 cm^{-1} and 1040 cm^{-1}, corresponding to Si-O-Si bonding.**Error! Bookmark not defined.** The characteristic band at ~574 cm^{-1} is associated with P-O bands [Fig.5.2]. FTIR spectra of NKN reveal the presence of the Nb-O octahedron peak at 524 cm^{-1} [1]. Overall, the FTIR spectra of BG-NKN composites corroborate well with those of the XRD results.

5.2 Mechanical properties

5.2.1 Hardness and fracture toughness

The densification of the sintered BG and BG – (10 - 30) NKN composite samples were measured to be 96.95 ± 0.46, 97.4 ± 0.41, 98.74 ± 0.31 and 96.97 ± 0.38 % with respect to the theoretical density of the samples. It can be noted that above a threshold of 20 vol. % NKN in BG, the densification of the composite is observed to decrease which subsequently, affects the mechanical and electrical response. Fig. 5.3 (a) shows the variation of Vickers hardness as well as fracture toughness for BG– x NKN (x = 0 - 30 vol. %) composites. The hardness values of pure BG, and BG – (10 - 30) NKN composites were obtained to be (0.23 ± 0.11), (3.58 ± 0.32), (4.06 ± 0.38) and (2.86 ± 0.112) GPa, respectively. Among the sintered samples, BG - 20 NKN shows the maximum hardness value, which can be associated with the highest densification of BG - 20 NKN among all the composites.

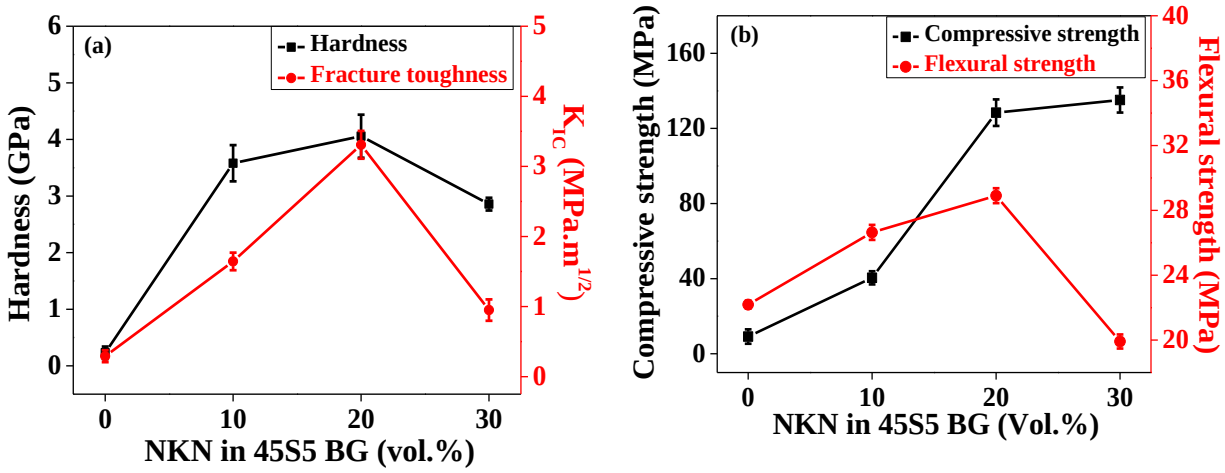

Fig. 5.3 Variation of mechanical properties of BG with addition of NKN (a) Hardness and Fracture toughness (K_{IC}), (b) Compressive and flexural strengths.

The fracture toughness of BG and BG – (10 - 30) NKN composites were calculated to be 0.30 ± 0.09, 1.64 ± 0.13, 3.31 ± 0.20 and 0.95 ± 0.15 MPa.m$^{1/2}$, respectively. The fracture toughness of BG has been significantly enhanced by the incorporation of NKN piezoelectric secondary phase in BG. Maximum fracture toughness was obtained for the BG - 20 NKN composition. Beyond this limit (> 20 vol. % NKN), the fracture toughness started to decrease with further addition of piezoelectric secondary phase. Liu et al. [2] demonstrated that the addition of up to 5 vol. % of lithium tantalate in alumina enhances the fracture toughness of the composite (upto 5.4 MPa.m$^{1/2}$). However, beyond 5 vol. % (threshold limit) addition leads to decrease in toughening effect. The piezoelectric toughening i.e., energy dissipation and domain switching has been suggested to provide additional toughening in such piezoelectric composite systems [3]. In a typical piezoelectric material, the dipoles are randomly oriented in a particular region, called domain, which is separated by another domain via domain boundary. When the propagating crack approaches the piezoelectric

secondary phase in the matrix, the dipoles tend to align in a particular direction, owing to the piezoelectric effect. In the process of dipole alignment, the crack dissipates energy which consequently, toughens the material [4]. Hwang et al. [5] demonstrated the domain switching of lead lanthanum zirconate titanate (PLZT) on the application of mechanical and electrical stimuli. The mechanical load deforms the crystals and changes the domain alignment by 90° (maximum) whereas, the electric field changes the domain alignment by 180° [5].

5.2.2 Compressive and flexural strengths

The compressive strength of the sintered BG and BG – (10 - 30) NKN composites were obtained to be 9.14 ± 3.84, 40.45 ± 3.51, 128.38 ± 7.06 and 135.15 ± 6.68 MPa, respectively [Fig. 5.3 (b)]. The addition of piezoelectric NKN secondary phase in 45S5 BG significantly enhances the compressive strength. The maximum compressive strength (135.15 ± 6.68 MPa) was obtained for BG - 30 NKN composite. The flexural strength of the sintered BG and BG – (10 - 30) NKN composite samples was obtained to be 22.19 ± 0.25, 26.64 ± 0.46, 28.91 ± 0.46 and 19.92 ± 0.44 MPa, respectively. The maximum flexural strength was obtained for BG-20 NKN composite system [Fig. 5.3 (b)]. The piezoelectric secondary phases dissipate the crack energy by their domain switching. The domain wall motion or domain switching of piezoelectric secondary phase has been suggested as one of the possible strengthening mechanisms [4]. It is well known that the compressive strength of the ceramics is generally higher. In addition, incorporation of NKN secondary phase in BG can produce more grain boundaries and hinder the dislocation movement which consequently, provide additional strength [6,7]. Beyond the threshold limit of secondary phase, relative density decreases and as a result, strength decreases despite of higher content of piezoelectric secondary phase [8]. For example, the addition of up to 5 vol. % of lithium tantalate in

alumina has been reported to enhance the flexural strength of the composite (upto 438 MPa). However, beyond 5 vol. % (threshold limit) addition leads to decrease in strengthening effect [2].

Overall, it is observed that the addition of piezoelectric NKN secondary phase in BG enhances the hardness, fracture toughness, compressive strength and flexural strength significantly.

5.3 Dielectric and electrical behavior

5.3.1 Dielectric measurement

Fig. 5.4 illustrates the variation of dielectric constant (ε_r) and loss tangent (D) with temperature for pure BG and BG – (10 - 30) NKN composites at few selected frequencies. At room temperature and 10 kHz of frequency, dielectric constant and loss for BG and BG - (10 - 30) NKN have been measured to be (13, 0.09), (15, 0.15), (13, 0.16) and (19, 0.11), respectively, which are comparable to the dielectric constant of natural bone (8-10) [9,10]. It is observed that the dielectric constant and loss values for monolithic BG are almost constant in the lower temperature (< 100ºC) region, irrespective of frequency [Fig. 5.4 (a)]. With further increase in temperature, ε_r and D increases with temperature. However, this increase in more prominent at lower frequencies than at higher frequencies. All the sintered BG - (10 - 30) NKN composite samples reveal almost similar dielectric behaviour [Figs. 5.4 (b), (c) and (d)]. Dipolar polarization can be suggested as one of the possible polarization mechanisms for such frequency dispersion in dielectric constant [Fig. 5.4] [11,12]. The hopping of the alkali ions (Na^+ ions) play an important role in governing the polarization in BG [13-16]. In BG, the hopping of Na^+ ions occurs by two ways. First, due to higher acidity of PO_4^{3-} ions, alkali Na^+ ions migrate towards the interstitial positions near the region of phosphate (PO_4^{3-})

or silicate ions to get more stable position [17] Secondly, Na^+ ions migrate due to the local distortion which create the free volume in BG glassy phase and allow the cationic movement [18].

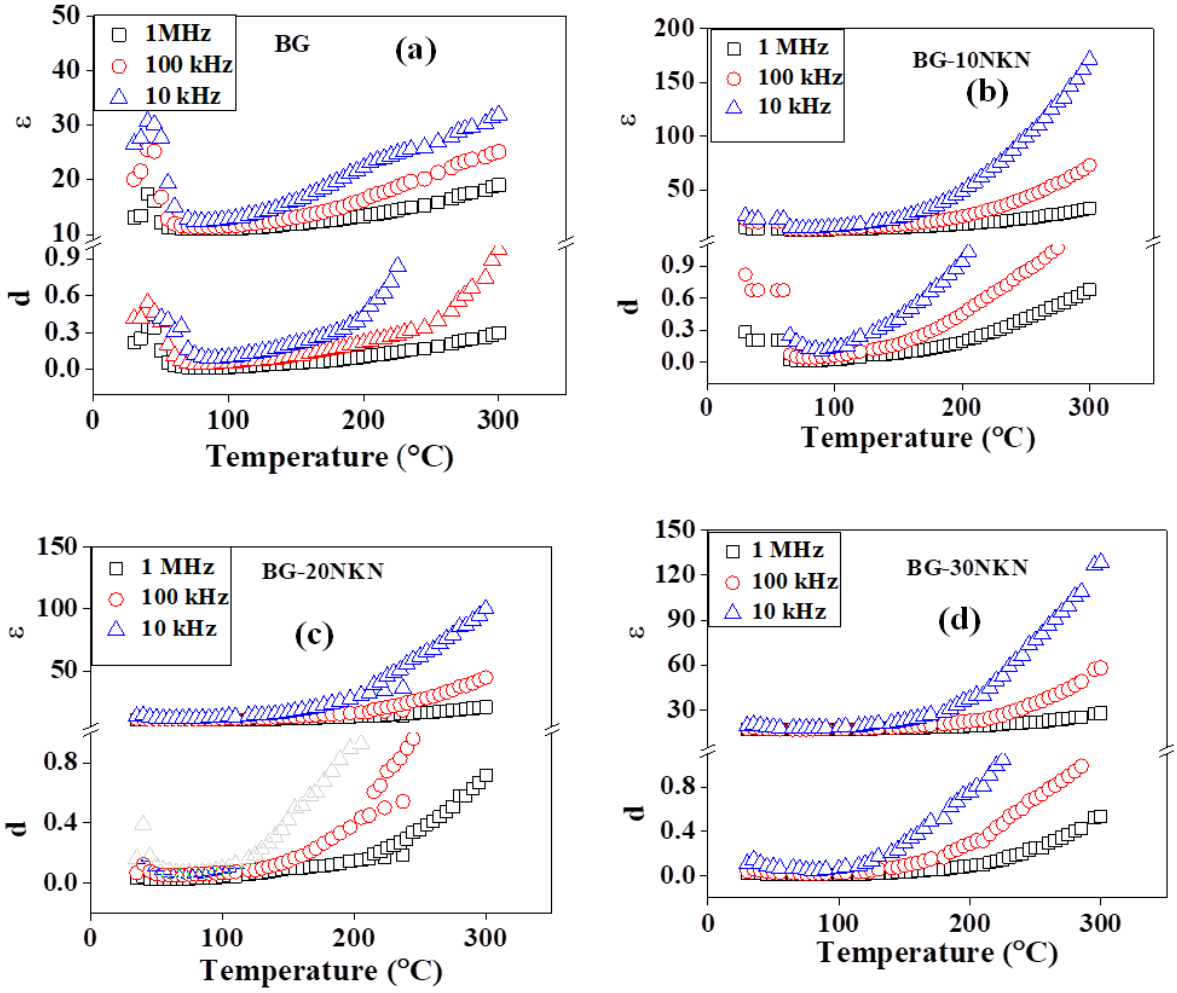

Fig. 5.4 Variation of dielectric constant and loss with temperature for (a) BG, (b) BG -10 NKN (c) BG - 20 NKN and (d) BG - 30 NKN at frequencies of 10 KHz, 100 kHz and 1 MHz, respectively.

Alkali metals (Sodium and Potassium) volatilized during sintering of NKN and superoxidation process occur during cooling of the sample in air atmosphere, due to which

conduction mode changes from ionic to electronic p type conduction (via holes) in grain boundary region, [19]

During sintering,

$$2\,M_M^{\times} + O_O^{\times} \leftrightarrow M_2O \uparrow + 2\,V_M^{'} + V_O^{\circ\circ} \qquad (5.1)$$

During cooling,

$$2\,V_M^{'} + V_O^{\circ\circ} + \frac{1}{2}O_2 \leftrightarrow 2\,V_M^{'} + O_O^{\times} + 2\,h^{\circ} \qquad (5.2)$$

Combining eqs. (1) and (2), one can obtain

$$2\,M_M^{\times} + \frac{1}{2}O_2(gas) \leftrightarrow M_2O(gas) + 2\,V_M^{'} + 2\,h^{\circ} \qquad (5.3)$$

Where, M denotes the alkali metal, V and h denote the vacancy and hole, respectively. However, the p type conduction decreases due to less volatilization of alkali metals and generation of the oxygen vacancies at reduced atmosphere suggest the n type conduction in the sintered samples [19].

$$O_O^{\times} \rightarrow \frac{1}{2}O_2 + V_O^{\circ\circ} + 2\,e^{'} \qquad (5.4)$$

The measured dielectric constant values of BG – (10 - 30) NKN composites have been compared with those of the values, calculated from the existing theoretical models [Fig. 5.5]. Dielectric constant of the samples were calculated using parallel and series Wiener bounds [20] as well as logarithmic mixture rule [21] as,

$$\varepsilon_{composite} = V_{BG}\varepsilon_{BG} + V_{NKN}\varepsilon_{NKN} \qquad (5.5)$$

$$\frac{1}{\varepsilon_{composite}} = \frac{V_{BG}}{\varepsilon_{BG}} + \frac{V_{NKN}}{\varepsilon_{NKN}} \qquad (5.6)$$

$$\log \varepsilon_{\tau} = \Sigma_i V_i \log \varepsilon_i \qquad (5.7)$$

Where, V and ε are the volume fraction of corresponding phase and dielectric constant, respectively.

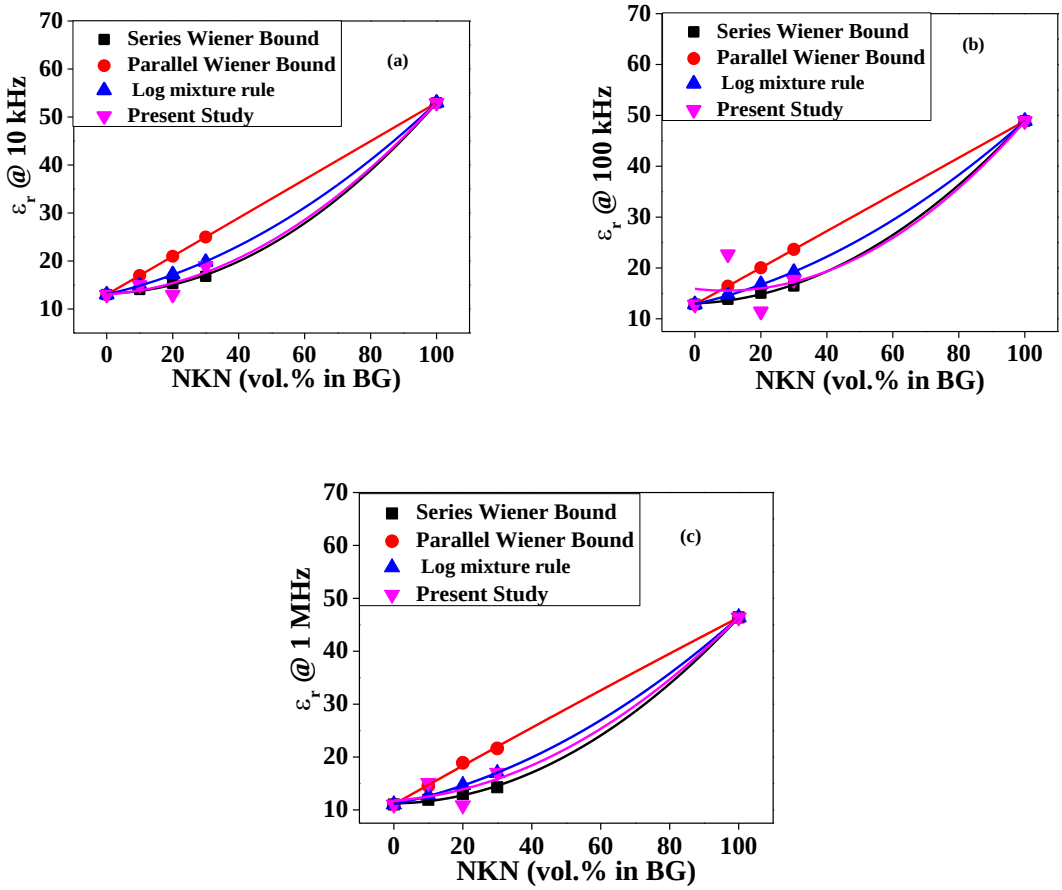

Fig. 5.5: Comparison of dielectric constant between parallel and series Wiener bounds, log mixture rule and present study at frequencies of (a) 10 kHz, (b) 100 kHz and (c) 1 MHz.

Newnham et al. [22] suggested that the connectivity between matrix and secondary phase influences dielectric and mechanical properties of the composites. For lower content of secondary phase, it can be connected with matrix phase via 0-3 connectivity. For 0-3 connectivity in the binary systems, Landauer suggested an expression as, [23]

$$\mathbf{F} = \mathbf{V_1}\frac{\boldsymbol{\varepsilon_1} - \boldsymbol{\varepsilon_c}}{\boldsymbol{\varepsilon_1} + \mathbf{2}\,\boldsymbol{\varepsilon_c}} + \mathbf{V_2}\frac{\boldsymbol{\varepsilon_2} - \boldsymbol{\varepsilon_c}}{\boldsymbol{\varepsilon_2} + \mathbf{2}\,\boldsymbol{\varepsilon_c}} \qquad (\mathbf{5.8})$$

Where, V_1 and V_2 are the volume fractions of the constituent phases. ε_1, ε_2 and ε_c are the dielectric constant of secondary phase, matrix and composite, respectively. It has been

reported that the value of F must be zero for perfect 0-3 connectivity [23]. From eq. 5.8, the calculated values of F for BG - (10 - 30) NKN composite system were 0.003, 0.101 and 0.122, respectively, at 10 kHz of frequency. The non-zero values of F indicate the higher level connectivity between NKN and BG phases. Jayasundere and Smith [24] suggested that with increase in the content of piezoelectric secondary phases in the composite, the interaction between piezoelectric phases takes place. For such condition, the following expression can be used to calculate the dielectric constant of composite,

$$\boldsymbol{\varepsilon} = \frac{\boldsymbol{\varepsilon_1 V_1} + \boldsymbol{\varepsilon_2 V_2}\left[\frac{\mathbf{3\varepsilon_1}}{\boldsymbol{\varepsilon_2 + 2\varepsilon_1}}\right]\left[\mathbf{1} + \frac{\mathbf{3V_2(\varepsilon_2 - \varepsilon_1)}}{\boldsymbol{\varepsilon_2 + 2\varepsilon_1}}\right]}{\mathbf{V_1} + \mathbf{V_2}\left[\frac{\mathbf{3\varepsilon_1}}{\boldsymbol{\varepsilon_2 + 2\varepsilon_1}}\right]\left[\mathbf{1} + \frac{\mathbf{3V_2(\varepsilon_2 - \varepsilon_1)}}{\boldsymbol{\varepsilon_2 + 2\varepsilon_1}}\right]} \qquad (\mathbf{5.9})$$

Using eq. 5.9, the dielectric constant values for BG – (10 - 30) NKN composites were calculated to be 15.38, 18.54 and 22.42, respectively. In case of polyphase ceramics, the effective dielectric constant of the samples can be calculated using the following expression [25],

$$\boldsymbol{\varepsilon_{eff}} = \frac{\boldsymbol{\varepsilon_m V_m}\left[\frac{\mathbf{2}}{\mathbf{3}} + \frac{\boldsymbol{\varepsilon_i}}{\mathbf{3\varepsilon_m}}\right] + \boldsymbol{\varepsilon_i V_i}}{\mathbf{V_m}\left[\frac{\mathbf{2}}{\mathbf{3}} + \frac{\boldsymbol{\varepsilon_i}}{\mathbf{3\varepsilon_m}}\right] + \mathbf{V_i}} \qquad (\mathbf{5.10})$$

Where, V_m, V_i, ε_m, and ε_i are the volume fraction and dielectric constant of matrix and secondary phase, respectively. The effective dielectric constants for BG – (10 - 30) NKN at 10 kHz (room temperature) were calculated to be 15.08, 17.39 and 19.98, respectively (using eq. 5.10). The measured values of dielectric constant for the BG - (10 - 30) NKN composites are deviated about 0.5, 33 and 5 % deviation with those of the calculated values.

5.3.2 AC conductivity measurement

Fig. 5.6 represents the variation of ac conductivity with frequency (1 kHz – 1 MHz) at few selected temperatures for monolithic BG and BG – (10 - 30) NKN composite system. It is observed that the ac conductivity of the sintered samples increases with frequency up to 200ºC after a lower frequency (1 Hz - 1 kHz) plateau region. For higher temperatures (> 200ºC), the plateau region appeared to shift towards higher frequency (10 kHz) range. At 500ºC, almost constant value of ac conductivity is observed in the measured frequency range. In the lower frequency region, a significant increase in conductivity with temperature is observed [15].

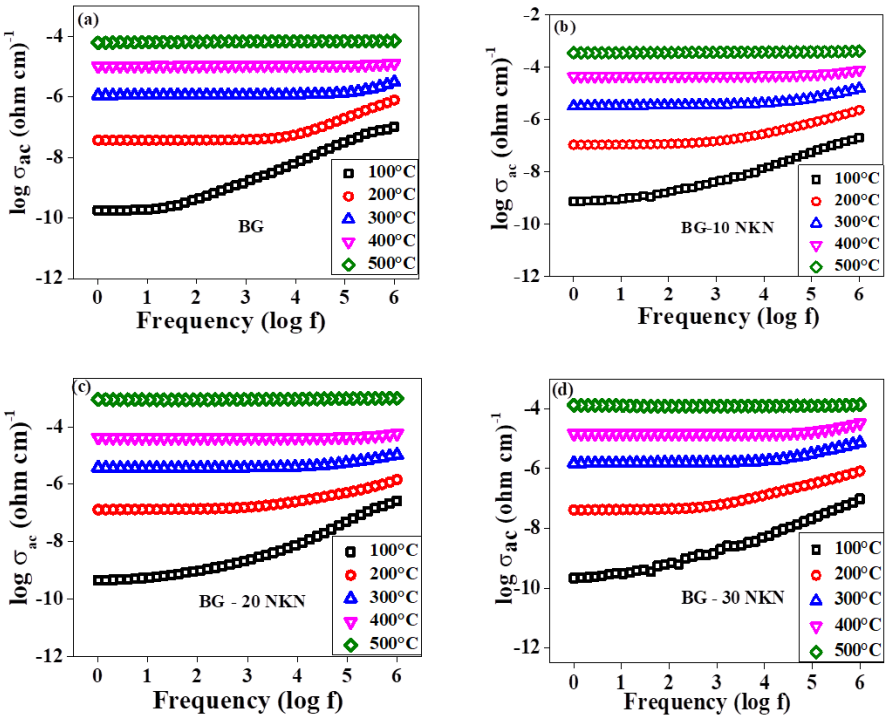

Fig. 5.6. Variation of log σ_{ac} with frequency at few temperatures for composites (a) BG, (b) BG - 10 NKN, (c) BG - 20 NKN and (d) BG - 30 NKN composites.

Below the glass transition temperature, the conduction is due to formation and migration of monovalent cationic vacancy or Na^+ ions. Whereas, the conduction above the glass transition

temperature is due to migration of free volume, created by local deformation in glassy phase.[15] The room temperature values of ac conductivity for BG – (10 - 30) NKN composite are measured to be 7.28×10^{-7}, 1.47×10^{-8} and 9.87×10^{-9} (ohm cm)$^{-1}$ respectively, at 10 kHz. The ac conductivity of the natural bone has been reported in the order of 10^{-10} (ohm cm)$^{-1}$.[26] It has been suggested that the concentration of mobile alkali ions in BG and hopping of the alkali cations (Na^{+}) through interstitial sites or holes are responsible for the electrical conduction in BG [27,28]. Kobayashi et al. [19] reported the volatilization of alkali ions and formation of oxygen vacancies during the sintering of NKN are one of the possible reasons for the observed conduction in NKN (eqs. 5.1 – 5.4).

5.3.3 Impedance Analyses

Fig. 5.7 shows the complex impedance plots i.e., Nyquist plot for BG and BG – (10 - 30) NKN composites at temperatures of 100ºC [Fig. 5.7(a)], 200ºC [Fig. 5.7(b)] and 300ºC [Fig. 5.7(c)] [29]. The Nyquist plot represents the contribution of grain and grain boundary in the terms of their respective resistances and capacitances. For the sintered composite samples, the centre of semicircular arc lies below the real impedance axis which shows the involvement of multiple relaxation processes [Fig. 5.7 (a, b and c)] [30]. Grain and grain boundary contributions are attributed in high and low frequency phenomenon, respectively [31]. The resistances of the grain and grain boundary have been obtained using Z - view software. Figs. 5.7 (d - f) illustrate the variation of grain and grain boundary resistances with inverse of temperature. Activation energy has been calculated from the slope of log (R_g, R_{gb}) and 1000/T plot. The activation energies of grain (E_g) and grain boundary (E_{gb}) resistances are calculated to be 0.59, 0.86, 0.94 and 0.76, 0.93, 1.06 eV, for BG- x NKN (10, 20 and 30 vol. %) composites, respectively. The calculated values of activation energies suggest that

the hopping of oxygen vacancies and alkali ions (Na^+) migration are the primarily responsible for conduction in BG – x NKN composite systems [26,19].

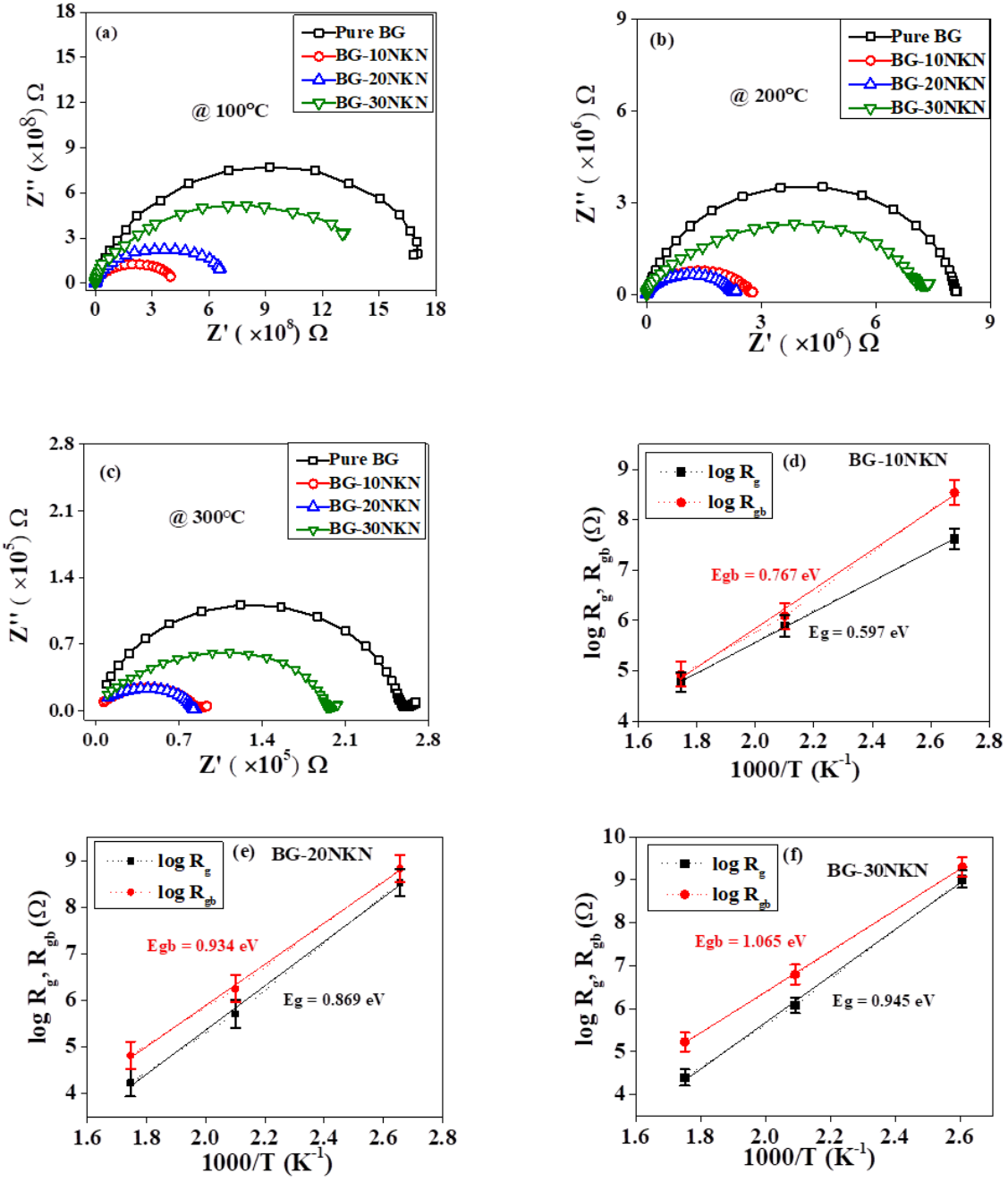

Fig. 5.7. Complex plane impedance plot for pure BG, BG - 10 NKN, BG - 20 NKN, BG - 30 NKN composites at temperature (a) 100˚C, (b) 200˚C, (c) 300˚C; (d), (e) and (f) represent the variation of log (R_g, R_{gb}) vs 1000/T

Fig. 5.8 represents the impedance and modulus spectroscopic behavior of BG, BG – (10 - 30) NKN composites, respectively which reveal the spectrum of conduction mechanisms [32,33]. The maxima of impedance and modulus spectroscopic plots are not positioned at the same frequency for all the measured samples, which suggest the long range as well as localized conduction in the samples [26]. Modulus spectroscopy shows the relaxation peaks which are shifted to the higher frequency region with increase in temperature and satisfy the relation $\omega.\tau = 1$, where, ω and τ are frequency and relaxation time, respectively [26].

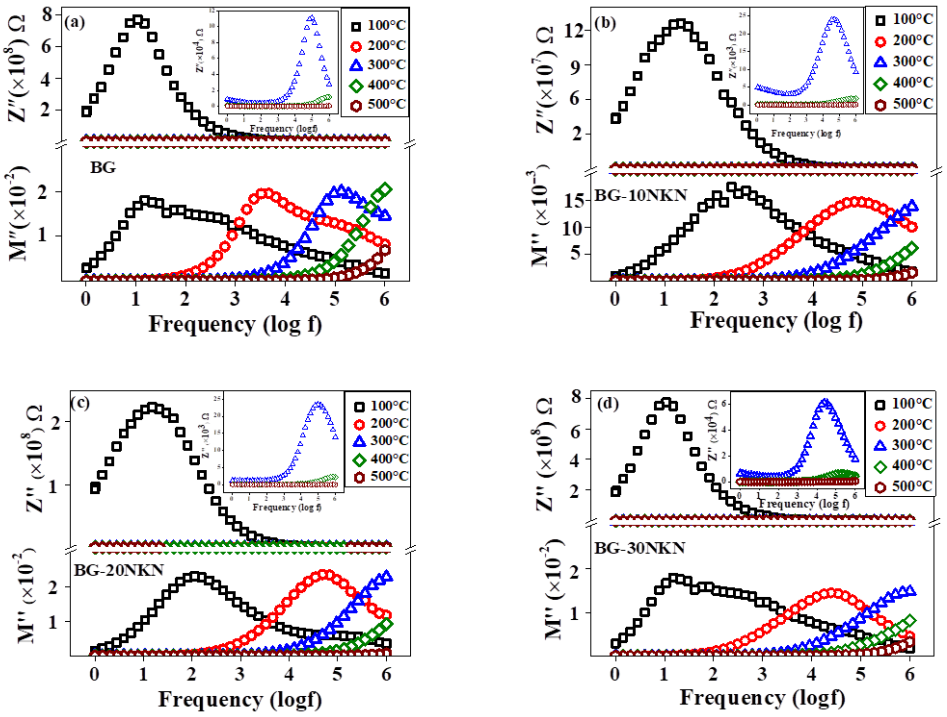

Fig. 5.8. Impedance and modulus spectroscopic plots for (a) BG, (b) BG - 10 NKN, (c) BG - 20 NKN and (d) BG - 30 NKN composites.

The variation in spectroscopic peaks suggests that hopping of the charge carriers (Na^+ ions and oxygen vacancies) due to thermal stimulation is the possible conduction mechanisms.

Space charge and dipolar polarization mechanisms are responsible for the variation of peaks with respect to the position and amplitude in frequency scale [Figs. 5.8 (a-e)]. During sintering of the samples, oxygen vacancies, alkali ions and other defects are created in NKN and BG due to which mobility of the space charge increases [19,18].

5.4 Antibacterial behavior

5.4.1 MTT assay

Fig. 5.9 shows the antibacterial response of unpolarized and polarized monolithic BG and BG – (10 - 30) NKN composite system against gram positive *(S. aureus)* [Fig. 5.9 (a)] and gram negative *(E. coli)* bacteria [Fig. 5.9 (b)]. It is observed that the mean optical density for both the bacterial cells decreases with addition of the piezoelectric NKN as the secondary phase in BG [Fig. 5.9]. Statistical analyses reveal the significant difference in mean optical density of uncharged, positively and negatively charged BG – (10 - 30) NKN composites than monolithic BG. Statistically significant reduction in the mean optical density of cells on unpolarized and polarized BG - (10 - 30) NKN composites are observed with respect to BG [represented as * in Fig. 5.9 (a)].

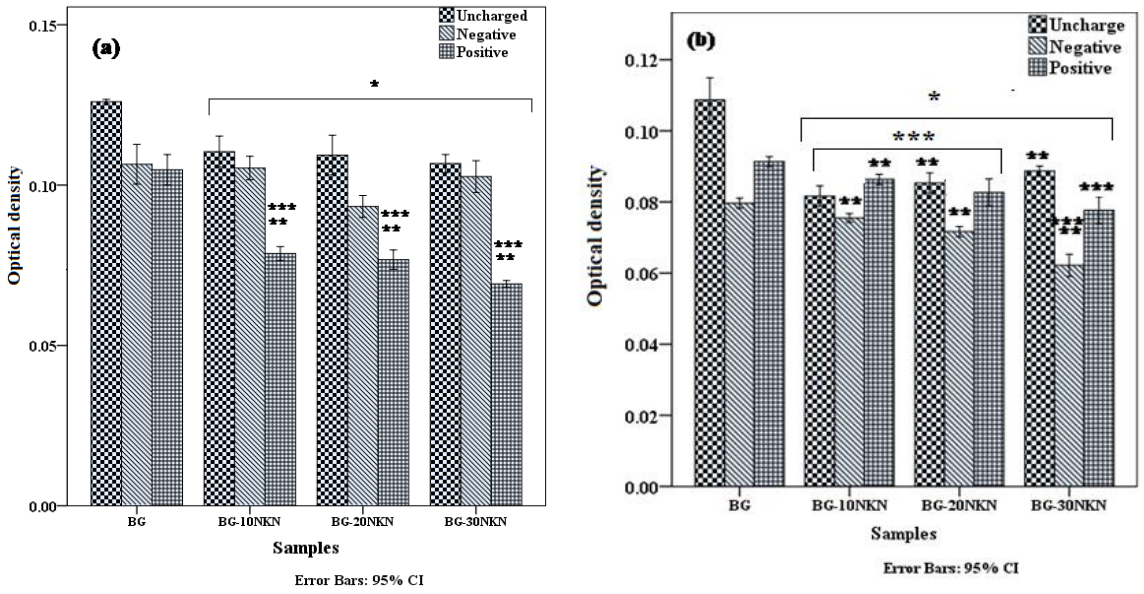

Fig. 5.9. Antibacterial response of unpolarized, positively and negatively polarized BG, BG - 10 NKN, BG - 20 NKN, BG - 30 NKN composites, against (a) gram positive (S. aureus) and (b) gram negative (E. coli) bacteria. Asterisk (*), (**) and (***) marks represent the significant difference in optical density of bacterial cells for the unpolarized, negatively and positively charged composite samples at $p < 0.05$, with respect to the monolithic BG.

As far as the influence of polarization on antibacterial response is concerned, positively charged BG - (10 - 30) NKN significantly decreases the mean optical density of *S. aureus* bacteria as compared to the negatively and positively charged BG [represented as ** and ***, respectively, in Fig. 5.9 (a)]. About 46 % population of *S. aureus* bacterial cells have been reduced on the positively charged surfaces of BG - 30 NKN composite samples. Similarly, for gram negative (*E. coli*) bacteria, the optical density of cells on BG - (10 - 30) NKN decreases with respect to those on uncharged BG [represented as * in Fig. 5.9 (b)]. Statistical analyses reveal that the mean optical density of *E. coli*, adhered on negatively charged surfaces of BG - (10 - 30) NKN composite significantly decreases with respect to negatively as well as positively charged BG [represented as ** and ***, respectively, in Fig.

5.9 (b)]. A layer of lipopolysaccharides and peptidoglycan in outer cell membrane of gram negative and gram positive bacteria, respectively, are reported to possess the negative charges [34,35]. Teichoic acids, embedded in peptidoglycan layer of gram- positive bacterial cell wall, are responsible for negative charge on the bacterial cell surface. The carboxylate and phosphate groups in teichoic acid contribute to the net negative charge [36]. Due to electrostatic interaction, negatively charged surface is expected to repel the bacterial cells and interact with positively charged surfaces of the sample [37]. The interaction of positively charged surfaces with bacteria has been reported to depolarize the cell membrane. Such depolarization leads to the abrupt change in the permeability of membrane which results in cell death. It has been suggested that the polarized surfaces increase the generation of reactive oxygen species (ROS) which induces antibacterial response [38]. ROS contains peroxides, superoxides, hydroxyl radical singlet oxygen, alpha oxygen etc. which are toxic in nature and damage the bacterial cells [39,40].

5.4.2 Kirby-Bauer test

Antibacterial response was also analysed in terms of zone of inhibition and colony formation using Kirby – Bauer test. In this test, firstly the equal bacterial suspension (50 μl) was seeded on nutrient agar plate. Following this, the polarized samples were placed onto culture so that positively, negatively and unpolarized surfaces of the samples were in direct contact with the culture. The samples were then incubated for 24 h at 37°C. After stipulated time period, culture plates were observed to evaluate the zone of inhibition in the vicinity of sample surface and images were captured using high resolution camera. Following this, a swab, below the sample surface was collected and transferred to fresh nutrient agar plates using sterile inoculation loop, and incubated further for 24 h at 37°C. After incubation, plates were

visually observed for colony formation [41]. Figs. 5.10 and 5.11 demonstrate the antibacterial response of polarized BG, BG – 10 NKN, BG – 20 NKN and BG – 30 NKN samples qualitatively for *S. aureus* and *E. coli* bacteria in terms of inhibition zone and colony formation, respectively, which were obtained using Kirby-Bauer method. It has been clearly observed that positively polarized samples illustrate larger zone of inhibition as compared to negatively polarized and unpolarized samples [Figs. 5.10 (e), (f), (g) and (h)].

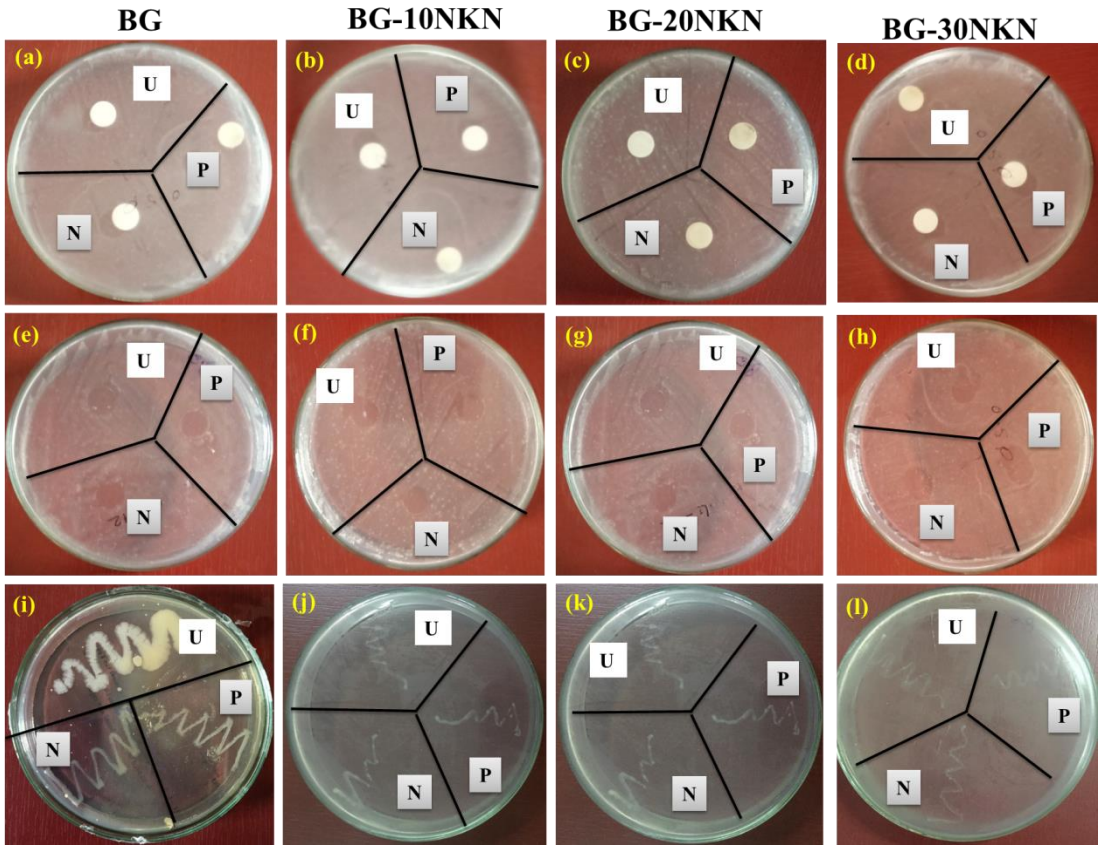

Fig. 5.10 Antibacterial response of unpolarized (U), negatively (N) and positively (P) polarized BG and BG-(10-30) NKN composite samples for S. aureus bacteria, observed using Kirby-Bauer method. (a), (b), (c) and (d) illustrate the cultured samples after 24 h of incubation in agar plate with S. aureus bacterial cells. (e), (f), (g) and (h) represent the area

under the incubated samples. (i), (j), (k) and (l) represent the colony formation (bacterial growth after transferring the swab from the area under the samples to a new agar plate).

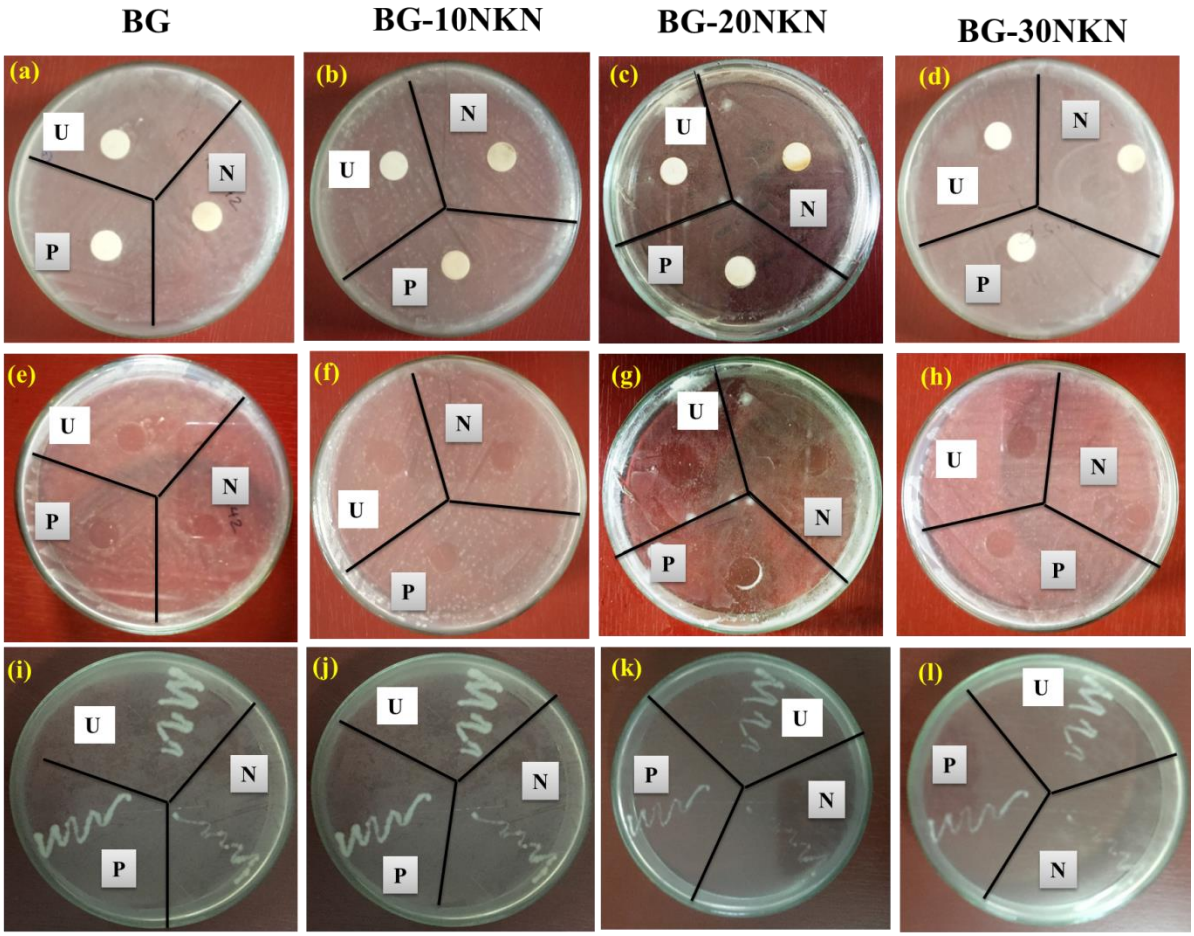

Fig. 5.11. Antibacterial response of unpolarized (U), negatively (N) and positively (P) polarized BG and BG-(10-30) NKN composite samples for E. coli bacteria, observed using Kirby-Bauer method. (a), (b), (c) and (d) illustrate the cultured samples after 24 h of incubation in agar plate with E. coli bacterial cells. (e), (f), (g) and (h) represent the area under the incubated samples. (i), (j), (k) and (l) represent the colony formation (bacterial growth after transferring the swab from the area under the samples to a new agar plate).

The transferred swab, in new plates, also shows no or very negligible bacterial colony for the swab collected beneath the positively polarized sample in comparison to negatively polarized and unpolarized samples [Figs. 5.10 (i), (j), (k) and (l)]. It can, therefore, be suggested that positively polarized samples offer more antibacterial response for *S. aureus*, irrespective of bioglass composition. While observing different bioglass compositions, it can also be suggested that BG – 30 NKN [Figs 5.10 (d), (h) and (l)] offers better antibacterial response as compared to BG [Figs. 5.10 (a), (e) and (i)], BG – 10 NKN [Figs. 5.10 (b), (f) and (j)] and BG-20 NKN [Figs. 5.10 (c), (g) and (k)] which reflects the efficacy of NKN itself as an antibacterial material. Similar behavior has been observed for negatively charged samples against gram negative (*E. coli*) bacterial cells. BG – 30 NKN [Figs. 5.11 (d), (h) and (l)] exhibit better antibacterial response than BG – 10 NKN [Figs. 5.11 (b), (f) and (j)] and BG – 20 NKN [Figs. 5.11 (c), (g) and (k)].

5.4.3 Live / dead ratio

Fig. 5.12 demonstrates the live/dead ratio for gram positive [Fig. 5.12 (a)] and gram negative [Fig. 5.12 (b)] bacterial cells on unpolarized and polarized BG and BG - (10 - 30) NKN composite samples. It has been observed that the live/dead ratio for both the bacterial cells decreases with addition of the piezoelectric NKN as the secondary phase in BG [Fig. 5.12]. The live/ dead ratio for unpolarized and polarized BG - (10 - 30) NKN composites are observed to be significantly decrease with respect to BG [represented as * in Fig. 5.12 (a)].

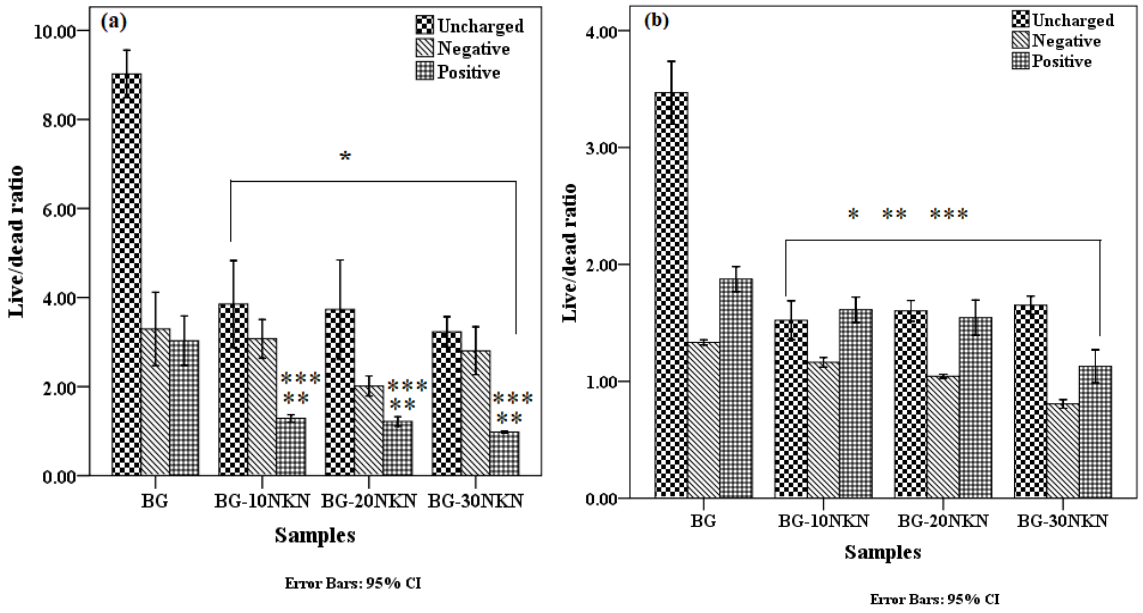

Fig. 5.12 Live/dead ratio for (a) gram positive (S. aureus) and (b) gram negative (E. coli) bacterial cells, cultured on unpolarized, negatively and positively polarized BG, BG - 10 NKN, BG - 20 NKN and BG - 30 NKN composites. Asterisk (*), (**) and (***) marks represent the significant difference in live/dead ratio for bacterial cells on the unpolarized, negatively and positively polarized composite samples at $p < 0.05$, with respect to the monolithic BG.

Irrespective of addition of secondary phase, polarization induced positively charged BG - (10 - 30) NKN significantly decreases the live/dead ratio for *S. aureus* bacteria as compared to the negatively and positively charged BG [represented as ** and ***, respectively, in Fig. 5.12 (a)]. Similarly, the live/dead ratio for gram negative (*E. coli*) bacteria, cultured on BG - (10 - 30) NKN composites decreases with respect to those on uncharged BG [represented as * in Fig. 5.12 (b)]. Statistical analyses reveal that live/dead ratio for *E. coli* on negatively charged surfaces of BG - (10 - 30) NKN composites significantly decreases with respect to

negatively as well as positively charged monolithic BG [represented as ** and ***, respectively, in Fig. 5.12 (b)].

5.4.4 Nitro blue tetrazolium (NBT) assay

Fig. 5.13 represents the superoxide production by gram positive [Fig. 5.13 (a)] and gram negative [Fig. 5.13 (b)] bacterial cells, cultured on unpolarized and polarized BG, BG – 10 NKN, BG – 20 NKN and BG – 30 NKN composites. Statistically significant difference in superoxide production can be clearly seen for BG – NKN composites as compared to BG.

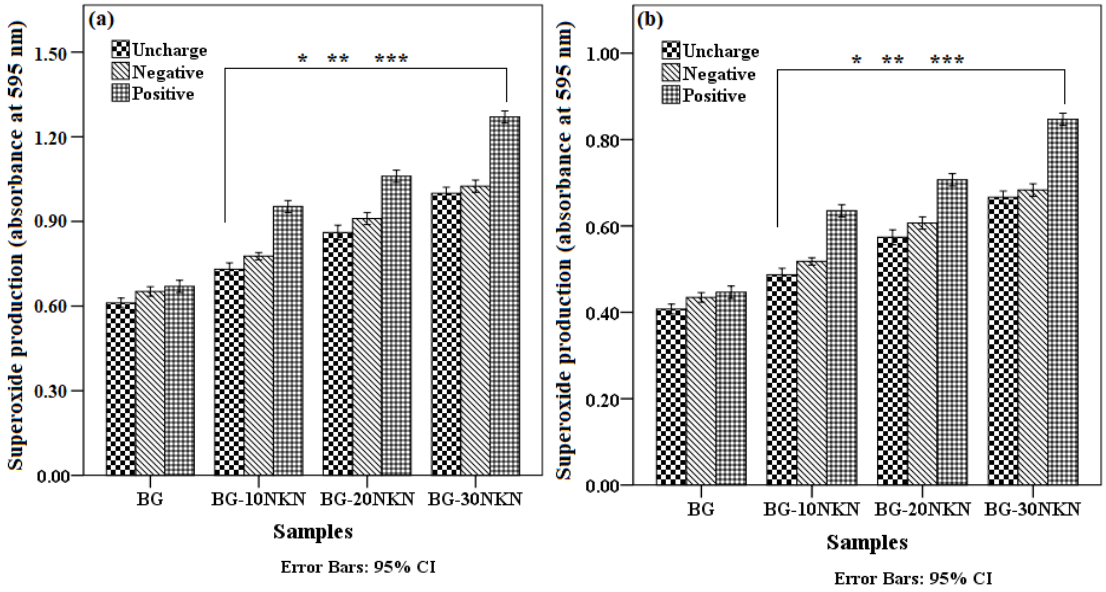

Fig. 5.13. Reactive oxygen species (superoxide), generated by (a) gram positive (S. aureus) and (b) gram negative (E. coli) bacterial cells, cultured on unpolarized, negatively and positively polarized BG, BG - 10 NKN, BG - 20 NKN, BG - 30 NKN composites. Asterisk (*), (**) and (***) marks represent the significant difference in superoxide production by the bacterial cells, cultured on the unpolarized, negatively and positively polarized composite samples at $p < 0.05$, with respect to pure BG.

The statistical analyses revealed that the superoxide production was enhanced on unpolarized and polarized BG - (10 - 30) NKN composite samples, in comparison to unpolarized and polarized BG samples (represented as *, ** and ***, respectively in Fig. 5.13). Besides this, the statistical significant difference in superoxide production was also increased on positively polarized surface in comparison to unpolarized and negatively polarized surfaces, irrespective of composition and bacteria type. It has been reported earlier that, electric field created due to polarization, induces the electrolysis of water, which leads to ROS generation.[42] Superoxide destabilizes ferrous (Fe^{2+}) ion by damaging iron–sulphur clusters in proteins present in bacterial cell which generate hydroxyl radicals by reacting with hydrogen peroxide (Fenton reaction, $Fe^{2+} + H_2O_2 \rightarrow Fe^{3+} + HO^{\bullet} + OH^-$) [43- 45]. These radicals generate oxidative stress which damage the cellular component of bacteria [46]. The ROS generation can be explained by the following equations [47],

$$\mathbf{H_2O + 2e^- \rightarrow H_2 + 2OH^-} \qquad \mathbf{(5.11)}$$

$$\mathbf{H_2 + 2\,H^- + 2e^- \rightarrow H_2O_2} \qquad \mathbf{(5.12)}$$

$$\mathbf{2H_2O \rightarrow O_2 + 4H^+ + 2e^-} \qquad \mathbf{(5.13)}$$

In addition, the polarized substrates increase the hydrophilicity of the surface, irrespective of their polarity [48]. Such increase in hydrophilicity also play an important role in reducing the bacterial adhesion [48].

5.5 *In vitro* cytocomapatibity

5.5.1 Cell Viability

Fig. 4.16 shows the MTT assay result for untreated and electric field (E-field) treated cells, cultured on BG and BG - 30 NKN, after 3, 5, and 7 days of incubation. The variation in value of mean optical density reflects the cells viability with respect to incubation period. It has been shown that unpolarized BG – 30 NKN have the statistically significant difference in cell viability as compared to monolithic BG. The statistical significant difference in cell proliferation was observed for 5 and 7 days cultured cells in comparison to cells, incubated for 3 days, irrespective of sample type and E-field treatment. It was also observed that negatively polarized surface promote cell proliferation in contrast to positively polarized and unpolarized surfaces, both in BG and in BG - 30 NKN. For 7 days of incubation, it has been observed that negatively charged BG – 30 NKN composite shows the maximum cell viability in terms of optical density. Also, within the same incubation period, the negatively charged BG - 30 NKN composite exhibits the higher cell viability in comparison to unpolarized and polarized pure BG sample. In addition, the cell viability further enhances by electrical stimulation for negatively polarized surface. Therefore, it is concluded that polarization along with external E-field, synergistically promote cell growth and proliferation.

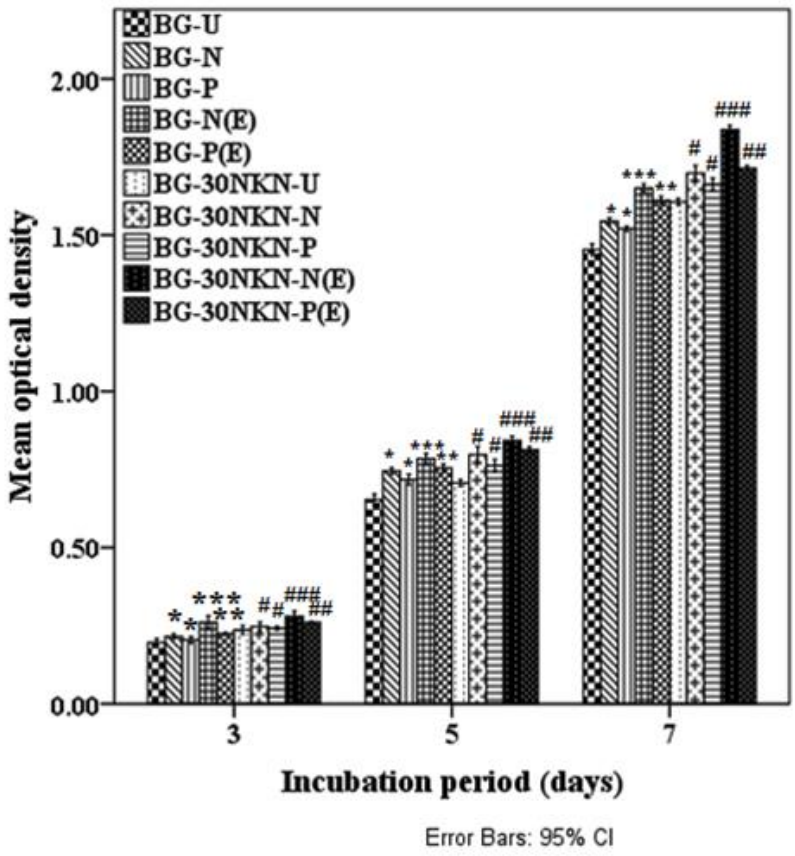

Fig.5.14. Combined effect of polarization and electric field treatment on viability of MG 63 cells, cultured on BG and BG-30 NKN composite. (*) and (#) represent the statistically significant difference in optical density for negatively and positively polarized BG and BG – 30 NKN composite with respect to unpolarized BG and BG – 30 NKN composite, (**) and (##) show the statistically significant difference in optical density for electric field treated positively polarized BG and BG – 30 NKN composite with respect to positively polarized BG and BG – 30 NKN composite and (***) and (###) show statistically significant difference in optical density for electric field treated negatively polarized BG and BG – 30 NKN composite with respect to negatively polarized BG and BG – 30 NKN composite.

It has been demonstrated by several researchers that polarization induced surface charge can enhance osteoblast cell proliferation and new bone formation [49–53] It was also reported

that the negatively polarized BG surface shows higher osteobonding ability in comparison to positively polarized surface [54-56] The cations like, Ca^{2+}, present in media were attracted towards negatively charged BG and promote the cell adhesion factors (integrin and fibronectin protein), which accelerate the cellular functionality [57]. The electrostatic interaction of Ca^{2+}, PO_4^{3-} ions with charged surface has been suggested as one of the possible reasons that facilitate cell adhesion and proliferation in vicinity of charged surface. In addition, external electrical stimulation further accelerate cell adhesion proliferation resulting increased cell density [58,59]. A number of studies revealed that the electrical stimulation open the voltage gated Ca^{2+} channel which promote the intracellular Ca^{2+} influx that enhances the cell proliferation [60- 62]. The influx of Ca^{2+} also activates Akt signaling pathway, that further promotes cell proliferation and inhibit cell apoptosis [63]. Thus, the activation of cell proliferation pathway as well as inhibition of apoptosis due to external electric field is another factor for higher osteoconductivity on electrically treated samples.

Overall, present study reveals that the addition of piezoelectric NKN secondary phase in BG improves the mechanical, electrical and dielectric behavior and antibacterial response as well as in vitro cytocompatibility of BG-NKN composite system.

5.6. Closure

BG - (10 - 30) NKN with high densification were synthesized by solid state synthesis route. Among all the developed compositions, BG - 20 NKN shows the maximum Vickers hardness, fracture toughness and flexural strength due to additional toughening and strengthening, provided by incorporation of piezoelectric NKN in BG. The dipolar polarization is observed as dominant polarization mechanism in the measured range of temperature and frequency. The complex impedance plots demonstrate the ionic conduction mechanism owing to, hopping of Na^+ ions and oxygen vacancies in BG - NKN composite. The addition of piezoelectric NKN secondary phase in BG improves the antibacterial behavior of BG - NKN composite against *S. aureus* and *E. coli* bacterial cells. Statistical analyses suggest that mean optical density on positively and negatively charged surfaces of BG - NKN composite significantly decreases the viability of gram positive (*S. aureus*) and gram negative (*E. coli*) bacterial cells. Irrespective of piezoelectric secondary phase, surface charge and electrical field further enhances the cell adhesion and growth for BG – 30 NKN. Overall, the incorporation of piezoelectric NKN in BG improves the electro-mechanical and polarization induced antibacterial behavior of BG.

References

1. D.Q. Zhang, Z.C. Qin, Yang XY, Zhu HB, Cao MS, "Study on synthesis and evolution of sodium potassium niobate ceramic powders by an oxalic acid-based sol–gel method," *Journal of Sol-Gel Science and Technology*. **57(1)** (2011) 31-35.

2. Y.G. Liu, D.C. Jia, Y. Zhou, "Microstructure and mechanical properties of a lithium tantalate-dispersed-alumina ceramic composite," *Ceramics International* **28** (2002) 111–114.

3. X.M. Chen, B. Yang, "A new approach for toughening of ceramics," *Materials Letters* **33** (1997) 37‑240.

4. W. Yang, T. Zhu, "Switch-toughening of ferroelectrics subjected to electric fields." *Journal of the Mechanics and Physics of Solids* **46(2)** (1998) 291-311.

5. S. C. Hwang, C.S. Lynch, R. M. McMeekingi, "Ferroelectric/ferroelastic interactions and a polarization switching model," *Acta Metallurgica et Materialia* **43(5)** (1995) 2073-2084.

6. T. E. Mitchell, K. P. D. Lagerlof, A. H. Heuer, "Dislocations in Ceramics," *Material Science and Technology* **1** (1985) 944-949.

7. D. Chen, M. E. Sixta, X. F. Zhang, L. C. DE Jonghe, R. O.Ritchie, "Role of the grain-boundary phase on the elevated-temperature strength, toughness, fatigue and creep resistance of silicon carbide sintered with al, b and c," *Acta materialia* **48** (2000) 4599–4608.

8. Y.G. Liu, D.C. Jia, Y. Zhou, "Microstructure and mechanical properties of a lithium tantalate-dispersed-alumina ceramic composite," *Ceramics International* **28** (2002) 111–114.

9. S. Singh, S. Saha, "Electrical Properties of Bone: A Review". *Clinical Orthopaedics and Related Research* **186** (1984) 249-271.

10. M.H. Shames, L.S. Lavine, "Physical bases for bioelectric effects in mineralized tissues". *Clinical Orthopaedics and Related Research* **355** (1964) 177-188.

11. G.B. Reinish, A.S. Nowick, Effect of Moisture on the Electrical Properties of Bone, *Journal of the Electrochemical Society*, **123(10)** (1976) 1451-145.

12. A.K. Dubey, B. Basu, K. Balani, R. Guo, A S. Bhalla, "Dielectric and Pyroelectric Properties of HAp-$BaTiO_3$ Composites," *Ferroelectrics* **423** (2011) 63–76.

13. A. Doi, "Comparison of frequency-domain and temperature domain electrical responses of ion-conductingg lass," *Solid State Ionics* **107** (1998) 81–88.

14. M.D. Ingram, "The impact of recent developments on the theory of and prospects for ionic conduction in glass," *Journal of Non-Crystalline Solids* **73** (1985) 247–253.

15. D. Ravaine, J.L.Souquet, "A thermodynamic approach to ionic conductivity in oxide glasses. Part 1. Correlation of the ionic conductivity with the chemical potential of alkali oxide in oxide glasses," *Physics and Chemistry of Glasses* **18(2)** (1977) 27–31.

16. M. Topic, A. Mogus-Milankovic, D. E.Day, "A study of polarization mechanisms in sodium iron phosphate glasses by partial thermally stimulated depolarization current," *Journal of Non-Crystalline Solids* **261** (2000) 146–154.

17. M.W.G Lockyer, D. Holland, R. Dupree, "NMR investigation of the structure of some bioactive and related glasses," *Journal of Non-Crystalline Solids* 188 (1995) 207–219.

18. J. L. Souquet, M. Duclot, M.Levy, "Ionic transport mechanisms in oxide based glasses in the supercooled and glassy states," *Solid State Ionics* **105** (1998) 237–242.

19. K. Kobayashi, M. Ryu, Y. Doshida, Y. Mizuno, C. A. Randall, "A Route Forwards to Narrow the Performance Gap between PZT and Lead-Free Piezoelectric Ceramic with Low Oxygen Partial Pressure Processed $(Na_{0.5}K_{0.5})NbO_3$," *Journal of the American Ceramic Society* **95 [9]** (2012), 2928–2933.

20. K. K. Karkkainen, A. H. Sihvola, K. I. Nikoskinen, “Effective permittivity of mixtures: Numerical validation by the FDTD method.” IEEE Trans. Geosci. Remote Sens. **38** (2000), 1303–1308.

21. W. D. Kingery, H. K. Bowen, D. R. Uhlmann, “Introduction to Ceramics,” Second Edition, John Wiley and Sons; (1976), 497.

22. R. E. Newnham, D. E. Skinner, L. E. Cross, “Connectivity and piezoelectric-pyroelectric composites.” *Materials Research Bulletin* **13** (1978), 525–536.

23. R. Landauer, “The electrical resistance of binary metallic mixtures.” *Journal of Applied Physics* **23** (1952), 779–784.

24. N. Jayasundere, B. V. Smith, “Dielectric constant for binary piezoelectric 0–3 composites.” *Journal of Applied Physics* **73** (1993), 2462–2466.

25. W. D Kingery, H. K. Bowen, D. R.Uhlmann, “Introduction to Ceramics,” 2nd ed. New York: Wiley Interscience, (1976), 948–949.

26. A.K. Dubey, Kakimoto K, Obata A, Kasuga T. Enhanced polarization of hydroxyapatite using the design concept of functionally graded materials with sodium potassium niobate, *RSC Advances* **4** (2014) 24601-24611.

27. J.E. Kelly III, J.F. Cordaro, M. Tomozawa,”Correlation effects on alkali ion diffusion in binary alkali oxide glasses,” *Journal of Non-Crystalline Solids*. **41(1)** (1980) 47-55.

28. H.J. Trap, J.M. Stevels, “Ionic and Electronic Conductivity of Some New Types' of Glass-Like Materials,” *Physics and Chemistry of Glasses* **4(5)** (1963); 193-205.

29. C. Bouzidi, N. Sdiri, A. Boukhachem, H. Elhouichet, M. Ferid, “Impedance analysis of $BaMo_{1-x}W_xO_4$ ceramics,” *Superlattices Microstructure*. **82** (2015), 559‑573.

30. I.M. Hodge, M.D. Ingram, A.R. West, "Impedance and Modulus Spectroscopy of polycrystalline solid electrolytes," *Journal of Electroanalytical Chemistry*, **74** (1976), 125-143.

31. X. Chen, Y. Wang, J. Chen, H. Zhou, L. Fang, L. Liu, "Dielectric Properties and Impedance Analysis of $K_{0.5}Na_{0.5}NbO_3$–$Ba_2NaNb_5O_{15}$ Ceramics with Good Dielectric Temperature Stability," *Journal of the American Ceramic Society*., **96 [11]** (2013), 3489–3493.

32. R. Rani, S. Sharma, R. Rai, A. L. Kholkin, "Investigation of dielectric and electrical properties of Mn doped sodium potassium niobate ceramic system using impedance spectroscopy," *Journal of Applied Physics*., **110** (2011) 104102.

33. A J Moulson, J M Herbert, "Electroceramics" Second addition, Wiley, (2003).

34. M Bellantone, NJ Coleman , L L Hench , Bacteriostatic action of a novel four-component bioactive glass, *Journal of Biomedical Materials Research.* **51(3) (**2000) 484-90.

35. E. Kłodzinska, M. Szumski, E. Dziubakiewicz, K Hrynkiewicz, E Skwarek, W Janusz, B. Buszewsk, "Effect of zeta potential value on bacterial behavior during electrophoretic separation," *Electrophoresis* **31** (2010) 1590–1596.

36. Y. Liu, R. Qin, SAJ Zaat, E. Breukink, M. Heger, "Antibacterial photodynamic therapy: overview of a promising approach to fight antibiotic-resistant bacterial infections" *Journal of Clinical and Translational Research* **1(3)** (2015) 140-167.

37. G. Harkes, J. Feijen and J..Dankert, "Adhesion of Escherichia coli on to a series of poly (methacrylates) differing in charge and hydrophobicity," *Biomaterials*, **12**, (1991), 853-860.

38. G. Tan, S. Wang, Y. Zhu, L. Zhou, P. Yu, X. Wang, T. He, J. Chen, C. Mao, C. Ning, "Surface-selective preferential production of reactive oxygen species on piezoelectric

ceramics for bacterial killing." *ACS applied materials & interfaces* **8 (37)** (2016) 24306–24309.

39. M.P. Murphy, A. Holmgren, N.G. Larsson, B. Halliwell, C.J. Chang, B. Kalyanaraman, S.G. Rhee, P.J. Thornalley, L. Partridge, D. Gems, T. Nyström, "Unraveling the biological roles of reactive oxygen species," *Cell metabolism,* (4), **13** (2011) 361-366.

40. X.Q. Chen, X.Z. Tian, I. Shin, J. Yoon, "Fluorescent and Luminescent Probes for Detection of Reactive Oxygen and Nitrogen Species," *Chemical Society Reviews* (9), **40** (2011)4783−4804.

41. W. Li, H. Wang, Y. Ding, E.C. Scheithauer, O.M Goudouri and A. Grünewald, "Antibacterial 45S5 Bioglass®-based scaffolds reinforced with genipin cross-linked gelatin for bone tissue engineering,"*Journal of Materials Chemistry* **3 (**2015) 3367-3378.

42. E. Serena, E. Figallo, N. Tandon, C. Cannizzaro, S. Gerecht, N. Elvassore, G. Vunjak-Novakovic "Electrical stimulation of human embryonic stem cells: cardiac differentiation and the generation of reactive oxygen species." *Experimental cell research* **315(20)** (2009) 3611–3619.

43. R.V. Lloyd, P. M. Hanna and R. P. Mason, "The origin of the hydroxyl radical oxygen in the Fenton reaction," *Free radical biology and medicine* **22 (5)** (1997) 885–888.

44. B. Blanc, C. Gerez, S. O. de Choudens, "Assembly of Fe/S proteins in bacterial systems: biochemistry of the bacterial ISC system," *Biochimica et Biophysica Acta (BBA)-Molecular Cell Research* **1853** (2015), , 1436–1447.

45. K. P. Singh, A. Zaidi, S. Anwar, S. Bimal, P. Das, V. Ali. "Reactive oxygen species regulates expression of iron–sulfur cluster assembly protein IscS of Leishmania donovani," *Free Radical Biology and Medicine* **75** (2014): 195-209.

46. P. Belenky, D. Ye Jonathan, C. BM Porter, N. R. Cohen, M. A. Lobritz, T. Ferrante, S. Jain. "Bactericidal antibiotics induce toxic metabolic perturbations that lead to cellular damage." *Cell reports* **13 (5)** (2015): 968-980.

47. M.R. Asadi and G. Torkaman, "Bacterial inhibition by electrical stimulation." *Advances in wound care* **3 (2)** (2014) 91−97.

48. A. K. Dubey, B. Basu. Pulsed electrical stimulation and surface charge induced cell growth on multistage spark plasma sintered Hydroxyapatite-Barium Titanate piezobiocomposite *Journal of the American Ceramic Society*, **97 [2]** (2014) 481–489.

49. D . Kumar , J.P. Gittings, I.G. Turner, C.R. Bowen, L.A. Hidalgo-Bastida, S.H. Cartmell, "Polarization of hydroxyapatite: Influence on osteoblast cell proliferation," *Acta Biomaterialia*, **6** (2010)1549-1554.

50. S. Itoh, S. Nakamura, M. Nakamura, K. Shinomiyaa, K. Yamashita, "Enhanced bone ingrowth into hydroxyapatite with interconnected pores by electrical polarization," *Biomaterials*, **27** (2006) 5572-5579.

51. S. Nakamura, T. Kobayashi, K. Yamashita, "Extended bioactivity in the proximity of hydroxyapatite ceramic surfaces induced by polarization charges," *Journal of Biomedical Materials Research* **61**(2002)593-599.

52. S. Itoh, S. Nakamura, M. Nakamura, K. Shinomiyaa, K. Yamashita, "Enhanced bone ingrowth into hydroxyapatite with interconnected pores by electrical polarization," *Biomaterials*, **27** (2006) 5572-5579.

53. S Itoh, S Nakamura, M Nakamura, K Shinomiya, K. Yamashita, "Enhanced bone regeneration by electrical polarization of hydroxyapatite," *Artif Organs* **3** (2006) 863–9.

54. T. Kobayashi, S. Nakamura, K. Yamashita, “Enhanced osteobonding by negative surface charges of electrically polarized hydroxyapatite,” *Journal of Biomedical Materials Research*, **57**(2001)477-484.

55. N.C. Teng, S. Nakamura, Y. Takagi, Y. Yamashita, M. Ohgaki, K. Yamashita, “A new approach to enhancement of bone formation using electrically polarized hydroxyapatite,” *Journal of Dental Research*, **80**(2001)1925-1292.

56. S. Nakamura, T. Kobayashi, K. Yamashita, “Numerical osteobonding evaluation of electrically polarized hydroxyapatite ceramics,” *Journal of Biomedical Materials Research A*, **68**(2004)90-94.

57. M. Ohgaki, T. Kizuki, M. Katsura, K. Yamashita, “Manipulation of selective cell adhesion and growth by surface charges of electrically polarized hydroxyapatite,” *Journal of Biomedical Materials Research* **57** (2001)366-373.

58. A.K. Dubey, S.D. Gupta, B. Basu, “Optimization of electrical stimulation parameters for enhanced cell proliferation on biomaterial surfaces,” *Journal of Biomedical Materials Research Part B: Applied Biomaterial*, **8B** (2011)18-29.

59. A. K. Dubey, B. Basu. Pulsed electrical stimulation and surface charge induced cell growth on multistage spark plasma sintered Hydroxyapatite-Barium Titanate piezobiocomposite *Journal of the American Ceramic Society*, **97 [2]** (2014) 481–489.

60. J. Tong, L. Sun, B. Zhu, Y. Fan, X. Ma, L. Yu, J. Zhang, “Pulsed electromagnetic fields promote the proliferation and differentiation of osteoblasts by reinforcing intracellular calcium transients,” *Bioelectromagnetics*, **38** (2017) 541-549.

61. M.Zhai, D. Jing, S. Tong, Y. Wu, P. Wang, Z. Zeng, G. Shen, X. Wang, Q. Xu, E. Luo, "Pulsed electromagnetic fields promote in-vitro osteoblastogenesis through aWnt/b-Catenin signaling-associated mechanism," *Bioelectromagnetics*, **37** (2016) 152-162

62. P. Zhou, F. He, Y. Han, B. Liu, S. Wei, "Nanosecond pulsed electric field induces calcium mobilization in osteoblasts," *Bioelectrochemistry*, **124** (2018) 7-12.

63. M.R. Love, S. Palee, S.C. Chattipakorn, N. Chattipakorn, "Effects of electrical stimulation on cell proliferation andapoptosis," *Journal of Cellular Physiology*, **233**(2018)1860-1876.